

Integrating non-contact surveys to characterize rock masses: the URLA case study

M. Janiszewski¹, S. Campagna², M. Torkan¹, G. Umili², L. Uotinen¹, A.M. Ferrero² & M. Rinne¹

¹ *Department of Civil Engineering, School of Engineering, Aalto University, Finland*

² *Department of Earth Sciences, University of Turin, Italy*

Abstract

This study investigates the integration of photogrammetry and laser scanning for rock mass characterization at the Underground Research Laboratory of Aalto University (URLA). The primary objective is to enhance our understanding of fracture properties at the test site using advanced non-contact geomechanical survey techniques.

High-resolution 3D models were generated to extract key fracture properties, including orientation, spacing, length, and persistence. The integration of photogrammetric and laser scanning data provided a detailed and accurate digital representation of the rock mass surface and fracture network, revealing significant spatial patterns through statistical analysis of fracture planes and traces.

The results demonstrate that semi-automatic mapping techniques produce reliable outcomes comparable to traditional manual surveys while significantly improving efficiency and measurement repeatability, thus reducing human bias. Statistical analysis provided robust insights into the spatial distribution and properties of fractures, demonstrating the potential of these non-contact methods in geological investigations. Trace mapping and intensity calculations quantified the degree of fracturing, highlighting variations in the degree of fracturing between tunnel sections.

These findings highlight the potential of non-contact geomechanical surveys with combined laser and photogrammetric 3D data for improving rock mass assessments, with future research focused on refining methodologies and expanding applications in complex underground environments.

Keywords

Non-contact survey methods; digital model; rock mass; tunnel; degree of fracturing

1 Introduction

When designing underground excavations and tunnels, it is essential to consider all the factors involved, such as geological structures, hydraulic and mechanical properties of the rock mass. The characterization of rock masses relies on the properties of the rock matrix and the discontinuities; the stability of rock spaces could almost depend on the discontinuities rather than on the strength of the intact rock (Hudson and Harrison 2000). Therefore, knowledge of the properties of discontinuities and their mapping in the context of underground rock mass characterization remains critical.

The traditional method of manually mapping discontinuities involves the use of a geological compass; its use requires the presence of the technician in close proximity to the rock face, exposing him or her to potential safety risks. In addition to those risks, the traditional method may face some problems, such as limited available time in the excavation stages, inaccessibility of some walls, and the influence of human error on the measurements (Gaich et al. 2003).

Non-contact techniques for mapping and extracting discontinuity features have been increasingly used in recent years (Ferrero et al., 2009; Gigli and Casagli 2011; Lato and Vöge 2012; Umili et al. 2013; Riquelme et al. 2014; Cao et al. 2017; Kong et al. 2020). They operate on Digital Surface Models (DSMs), which are reconstructed by generating high-resolution 3D point clouds using Structure-from-Motion (SfM) photogrammetry and laser scanners (Uotinen 2018).

Thanks to the increasing quality of digital images and the development of SfM software, it is possible to reproduce digital models with millimetre accuracy, thus minimizing errors and overcoming the limitations of traditional measurements, namely the possible inaccessibility of some walls or portions of them and the safety of technicians.

The research presented here was carried out in the Underground Research Laboratory of Aalto University (URLA). The objective of this study was to set up a photogrammetric survey along two converging tunnel walls in order to obtain a very high-resolution DSM, on which it was possible to apply different non-contact geomechanical survey methods and compare their results in terms of orientation data with those of the detailed traditional survey carried out on the same tunnel wall. In addition, the study focused on the assessment of the parameters that quantify discontinuity abundance in a rock mass: they are defined as the ratio between the dimension of the considered discontinuity feature and the sampling region's size (Dershowitz and Herda 1992; Mauldon and Dershowitz 2000). Different methods were applied to estimate these descriptors of the degree of fracturing of the rock mass and compare them.

2 Methodology

The URLA laboratory is located in southern Finland, on the campus of Aalto University in Otaniemi. The laboratory comprises a series of underground tunnels used for research and education at Aalto University. The study area is located approximately 20 m below ground level, at an intersection between Tunnel 11 and Tunnel 10 (Fig. 1). The site is situated in the Southern Finland plutonic suite, which consists mainly of plutonic rocks, but hypabyssal and metamorphic rocks are also present as described by the Geological Unit Report GTK (Nironen, 2024). In particular, the area lies within granodiorite rocks; locally there are lenses of metamorphic rocks such as gneisses, schists, and amphibolite. This area is affected by the intersection of several discontinuity sets that are also recognizable on the rock outcrops along the tunnel walls.

The first part of this study was the photogrammetric digitization of the portions of the two intersecting tunnels under investigation. The process consisted of two main steps: image acquisition and SfM photogrammetric reconstruction. A Canon EOS 5DS R camera with a 14 mm Canon lens was used to acquire images. The camera was set to F11 aperture, ISO 250, and RAW file format, placed on a tripod, and connected to a remote control to avoid possible image blurring. To best illuminate the rock face, two DeWalt DCL074 battery-powered lights were used in addition to the normal lighting inside the tunnel, and these were moved during the various shots to create homogeneous lighting conditions (Fig. 1).

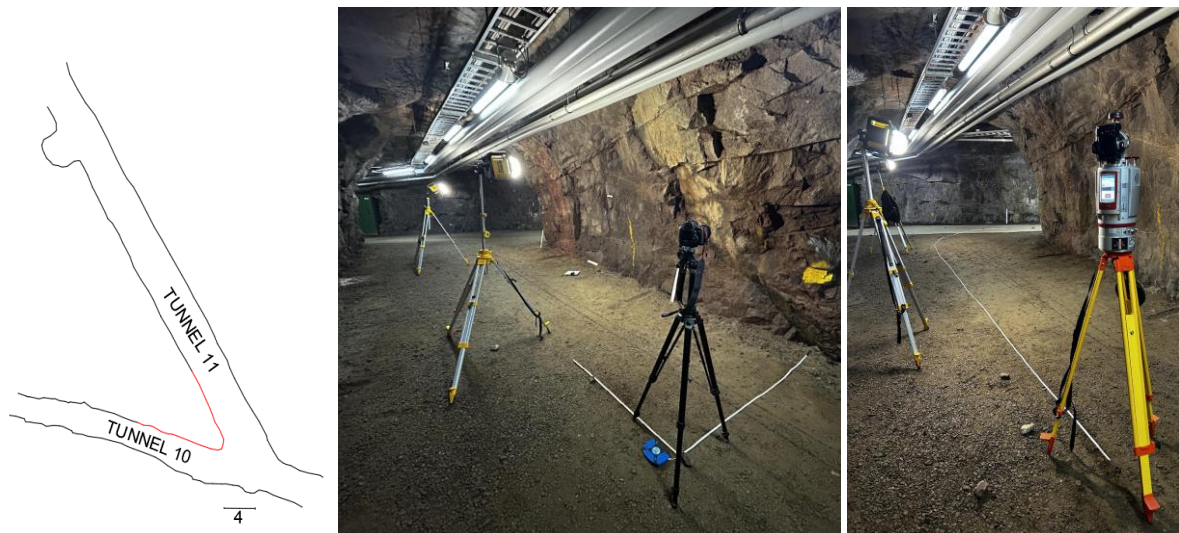


Fig. 1 Intersection of tunnel 11 and tunnel 10, the part of the tunnel subject of the research is shown in red (Left). Camera with lens and tunnel lighting set-up (Middle). Laser scanner RIEGL VZ400i (Right).

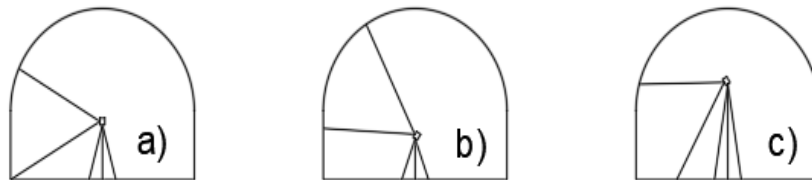


Fig. 2 a) Camera position in the first set of photos. b) Changing position to capture details of the roof. c) Changing position to capture details of the basal part.

In total, 72 photos were taken using the following procedure:

- Place the camera on the tripod, making sure that it is parallel to the wall in question, at 2 m from it.
- Take the first series of photos along the surface of the wall, always keeping the camera parallel to the wall (Fig. 2a), at regular intervals of 1 m to achieve an 80-90% lateral overlap between the photos.
- Take two more rows of photos in the same way but change the camera angle and tripod height to capture the roof (Fig. 2b) and the lower part of the wall (Fig. 2c), longitudinal overlap is 80%.

Once the images were captured, they were fed into the RealityCapture 1.4 software for performing the processing and reconstruction of the 3D model. The images were imported and aligned. The model was then scaled using special scale bars previously placed on the wall to define the distance between two distinct points that are visible in the images. The software then reconstructed a dense 3D point cloud and coloured it by applying a texture to the model.

The second procedure used for creating a 3D digital model of the same area was laser scanning. The process was divided into two main parts: laser scanning of the tunnel section in question and data processing using special software. A RIEGL VZ400i laser scanner (Fig. 1) was used for the scanning, which also allows the integration of a DSLR camera for point cloud colouring.

The laser scanner was set to high resolution to obtain a model with as much detail as possible. Again, DeWalt DCL074 lamps were used to provide lighting for the photos. The laser scanner was placed on a tripod for the best possible scanning, 15 scans were taken at 2 m intervals, taking approximately 7 minutes per scan position.

Once all the necessary scans had been acquired, they were entered into the RISCAN PRO 2.0 software for processing and reconstruction of the 3D model. As a first step, the software processed each scan individually, creating single 3D point clouds, and then it produced an overall point cloud by merging them.

Once the 3D digital models have been produced using the two methods, a point cloud editing software was used to analyse the two models separately or to combine them. In this case, CloudCompare v2.13.2 was used to produce a single digital model with a higher resolution than the two models taken separately. Higher resolution corresponds to a larger point density of the surface and, therefore, greater details of the discontinuity features.

Semi-automatic mapping of discontinuities was performed using the Discontinuity Set Extractor (DSE) software, developed by Riquelme et al. (2014). The DSE calculates the normal vectors of each point that is coplanar with neighbouring points and represents them as poles in a stereonet. Next, it calculates the density of the poles, and those that are considered most representative are extracted as discontinuity sets (Janiszewski et al. 2020). The point cloud is then segmented into discontinuity planes belonging to different sets. The orientation of the different sets is then calculated. The DSE also allows measurement of the spacing and persistence of the extracted discontinuity sets (Riquelme et al. 2015, 2018). The CloudCompare v2.13.2 software was used to calculate the length and aperture parameters, where the 'distance' function allows the distance between points to be measured.

3 Results and discussion

3.1 3D models of the tunnel sections

The point cloud obtained by photogrammetry consists of 17 634 175 points: for better visualisation, it was divided into two parts, one illustrating the wall section in Tunnel 10 (Fig. 3) and one the wall section in Tunnel 11 (Fig. 4). The point cloud generated by the laser scanner has 6 227 849 points. The merging of the point clouds obtained with photogrammetry and laser scanner was done using CloudCompare v2.13.2, and the resulting point cloud has a number of points equal to the sum of the two clouds, which is too high to be processed by the DSE software. Therefore, we chose to simplify it using the subsample point cloud function, with a spatial function set to 0.007 m.



Fig. 3 High-resolution point cloud in the Tunnel 10 section.



Fig. 4 High-resolution point cloud in the Tunnel 11 section.

3.2 Semi-automatic extraction of discontinuity sets

For the analysis by DSE, some sampling windows were selected along the tunnel area involved in the study, the same windows were digitally measured with Compass plugin in CloudCompare v2.13.2, and manual measurements with a geological compass.

The analysis window was obtained from the segmentation of the point cloud, then saved in ASCII format and imported into the DSE software. Statistical analysis was performed by setting the minimum angle between pole vectors to 30° and the number of principal planes to 5. From the extracted results, the DSE extracted four different coloured sets of discontinuities (Fig. 5). It is important to highlight that set J4 corresponds to the blast-induced fracture parallel to tunnel wall orientation due to the drill and blast excavation method.

The results of the semi-automatic (around 90 000 poles), digital (26 poles), and manual (35 poles) fracture mapping are compared in Fig. 6. The same sets of discontinuities were identified by the semi-automatic method (Fig. 6a-b) as by the digital method (Fig. 6c) and the geological compass (Fig. 6d), i.e., three sets of discontinuities plus a fourth representing the orientation of the front. Comparable results are obtained from all the methods used, as shown in Table 1.

The critical aspect of this comparison lies in the reliability of the measurements of the semi-automatic method, which leads to a significant reduction in the time required for the measurements of large data sets; clearly, the quality of the measurements is directly proportional to the quality, density, and completeness (i.e., absence of voids) of the point cloud.

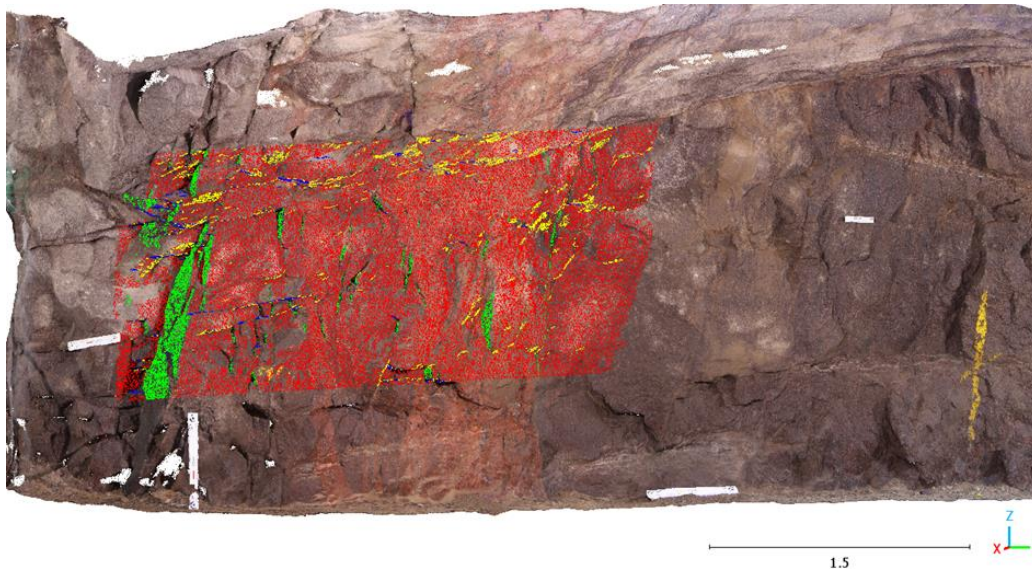


Fig. 5 Point cloud of part of Tunnel 11 with characteristic mapping window, discontinuities identified and coloured used DSE software. J1 = blue; J2 = green; J3 = yellow; J4 = red.

Table 1 Comparison of orientation results.

| METHOD | J1 | J2 | J3 | J4 |
|---------------------|--------|--------|-------|--------|
| Manual measurement | 12/149 | 82/144 | 43/17 | 82/238 |
| Digital measurement | 13/169 | 81/131 | 48/20 | 86/244 |
| DSE | 10/134 | 86/319 | 43/21 | 87/230 |

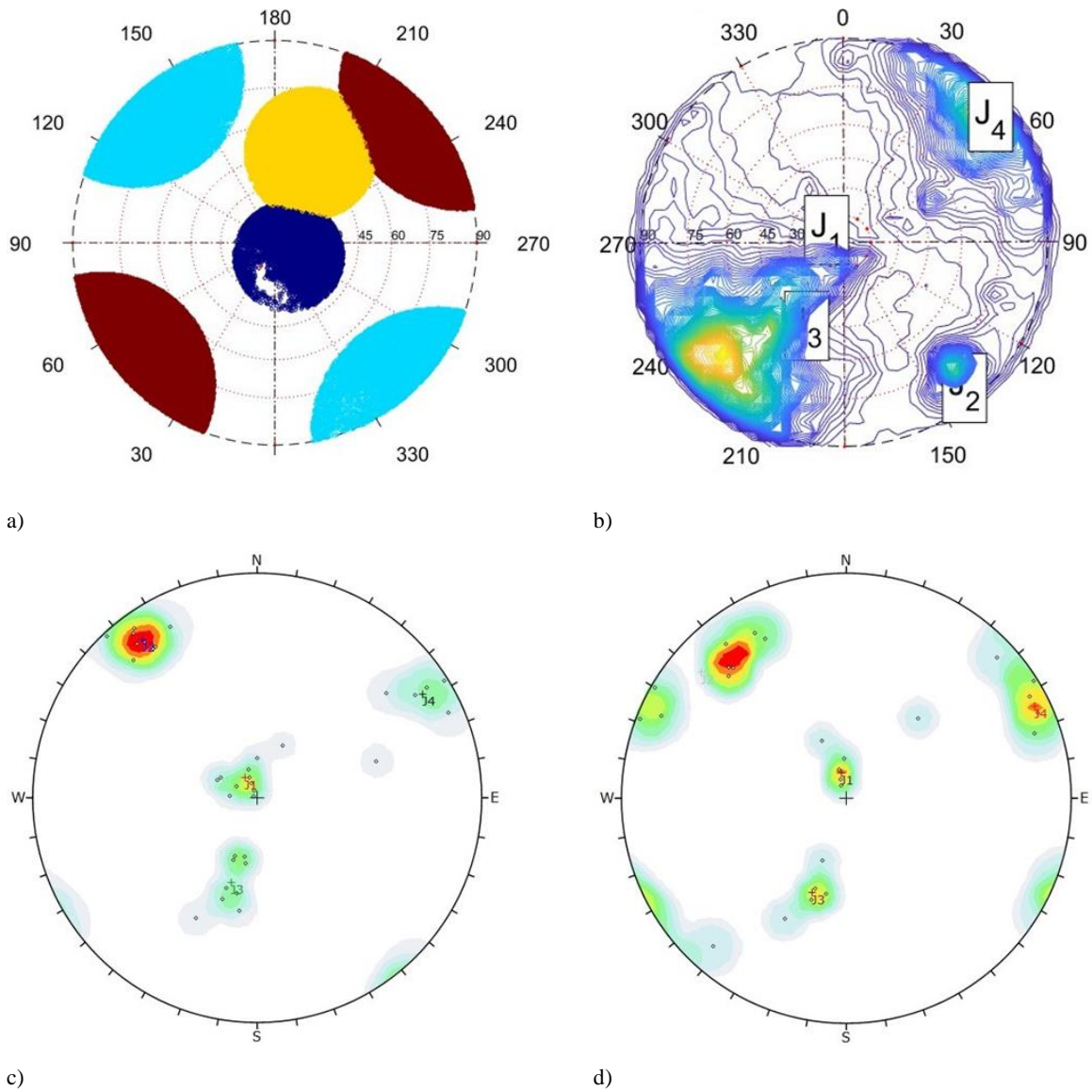


Fig. 6 a) DSE Assigned Poles b) DSE Poles Density c) Dips Poles density obtained with Manual measurement d) Dips Poles density obtained with Digital measurement.

3.3 Trace mapping and sampling

Once the trace map was created by manually identifying traces on the point clouds, circular window sampling (Zhang and Einstein 1998) was used to calculate two descriptors of the rock mass degree of fracturing, namely P_{21} and P_{32} . The areal intensity P_{21} is defined as the length of traces per unit sampling area. The volumetric intensity P_{32} is the area of fractures per unit volume of rock mass.

Two circular sampling windows were created and used, one along the wall of Tunnel 10 (Fig. 7a) and one along the wall of Tunnel 11 (Fig. 7b), the radius of the windows being 0.92 m and 1.29 m, respectively. The trace sampling procedure is based on a count of the classified traces in the considered sampling window. In fact, for each window, traces with both ends outside the window (N_0), traces with both ends within the window (N_2), and traces with only one end within the window (N_1) are counted separately. The trace count is reported in Table 2.

Table 2 Results of trace sampling and classification on circular window.

| | N_0 | N_2 | N_1 | N_T |
|-----------|-------|-------|-------|-------|
| Tunnel 10 | 3 | 12 | 7 | 22 |
| Tunnel 11 | 4 | 20 | 10 | 34 |

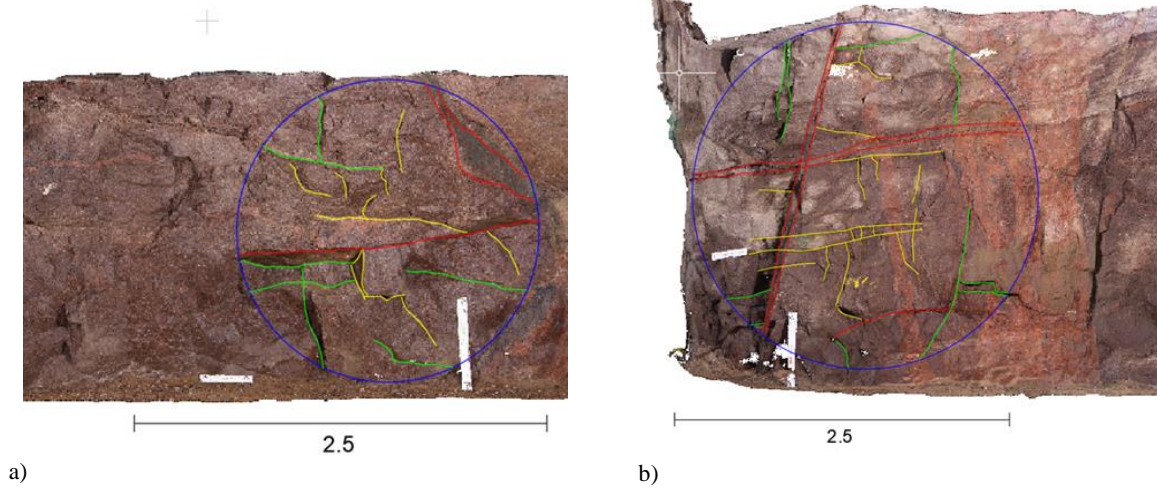


Fig. 7 Sampling windows a) in Tunnel 10, b) Tunnel 11. Green line = N, red line = N_0 , yellow line = N_2 .

For discontinuities assumed to be planar and with a circular shape, Zhang and Einstein (2000) proposed equations for calculating the mean trace length μ_l and its standard deviation σ_l based on a circular window of radius c :

$$\mu_l = \frac{\pi(N + N_0 - N_2)}{2(N - N_0 + N_2)} c \quad (1)$$

$$\sigma_l = \mu_l \cdot (COV)_m \quad (2)$$

where $(COV)_m$ is the coefficient of variation of the measured trace lengths.

Zhang and Einstein (2000) proposed to calculate the mean fractures area per unit volume of the rock mass as:

$$P_{32} = \frac{N_T E(A)}{V} \quad (3)$$

where N_T is the total number of sampled discontinuities, $E(A)$ is the mean discontinuity area calculated with equation (4) and V is the unit volume.

$$E(A) = \int_0^{\infty} \frac{\pi}{4} D^2 g(D) dD = \frac{\pi}{4} E(D^2) = \frac{\pi}{4} [E(D)^2 + V(D)] \quad (4)$$

The same authors proposed the equations to calculate the mean diameter $E(D)$ and the variance $V(D)$ to be used in Eq. 4, assuming a Gamma distribution as the best fitting one for the trace sample:

$$E(D) = \frac{64\mu_l^2 - 3\pi^2(\mu_l^2 + \sigma_l^2)}{8\pi\mu_l} \quad (5)$$

$$V(D) = \frac{[64\mu_l^2 - 3\pi^2(\mu_l^2 + \sigma_l^2)][3\pi^2(\mu_l^2 + \sigma_l^2) - 32\mu_l^2]}{64\pi^2\mu_l^2} \quad (6)$$

The results of this procedure applied on the two circular sampling windows are reported in Table 3. From the results obtained, the two survey windows obtain a very similar P_{21} index, while the P_{32} index is different, indicating a more fractured part of the rock mass. The higher P_{32} value in Tunnel 10 likely reflects increased joint density and excavation-induced fracturing, influenced by differences in tunnel orientation relative to pre-existing discontinuities and ground surface.

Table 3 Results of Zhang and Einstein method.

| | μ_l | σ_l | E(D) | V(D) | E(A) | P_{32} | P_{21} |
|-----------|---------|------------|------|------|------|----------|----------|
| Tunnel 10 | 0.61 | 0.44 | 0.45 | 0.14 | 0.27 | 2.25 | 4.49 |
| Tunnel 11 | 0.73 | 0.75 | 0.09 | 0.08 | 0.07 | 0.44 | 4.58 |

4 Conclusion

This study demonstrates the effectiveness of integrating photogrammetry and laser scanning for non-contact geomechanical surveys, as applied in Aalto University's Underground Research Laboratory URLA. High-resolution 3D models of tunnel walls captured detailed spatial data on rock fractures, enabling characterization of fracture properties such as fracture orientation. Four discontinuity sets and their orientations were extracted using digital mapping tools.

The semi-automatic methods showed reliability comparable to traditional manual mapping. This approach addresses limitations of traditional methods, such as accessibility challenges and human error, offering a robust and fast alternative for geological investigations.

Trace mapping and sampling enabled statistical analysis of the fracture spatial extent and the degree of fracturing in both tunnel sections. The results indicated a comparable areal intensity P_{21} in both tunnel sections and a higher volumetric intensity P_{32} in section 10 indicating a higher degree of fracturing. The extracted fracture properties, including spacing, trace length, and intensity (P_{21} , P_{32}), provide valuable input for rock mass classification factors such as RQD and J_n , with potential for further integration into non-contact geomechanical assessments. Future research will focus on refining these methods and expanding their application to diverse geological contexts and more demanding underground conditions.

References

- Cao T, Xiao A, Wu L and Mao L (2017) Automatic fracture detection based on Terrestrial Laser Scanning data: A new method and case study *Comput. Geosci.* 106 209–16
- Dershowitz WS, Herda H (1992) Interpretation of Fracture Spacing and Intensity. *Proc. 33rd U.S. Symp. on Rock Mechanics*, Santa Fe, New Mexico, pp 757-766.
- Ferrero A, Forlani G, Roncella R, Voyat H (2009) Advanced geostructural survey methods applied to rock mass characterization. *Rock Mechanics and Rock Engineering* 42,631–665.
- Gaich A, Fasching A, Schubert W (2003) Improved site investigation Acquisition of geotechnical rock mass parameters based on 3D computer vision. In: Beer G. (eds) *Numerical Simulation in Tunnelling*. Springer, Vienna. https://doi.org/10.1007/978-3-7091-6099-2_3
- Gigli G and Casagli N (2011) Semi-automatic extraction of rock mass structural data from high resolution LIDAR point clouds *Int. J. Rock Mech. Min. Sci.* 48 187–98
- Hudson J and Harrison J (2000) *Engineering Rock Mechanics: An Introduction to the Principles*. 2nd edn. Elsevier Science, Oxford, UK.
- Janiszewski M, Uotinen L, Rinne M and Baghbanan A (2020) Digitisation of hard rock tunnel for remote fracture mapping and virtual training environment In *ISRM International Symposium EUROCK 2020*.
- Kong D, Wu F and Saroglou C (2020) Automatic identification and characterization of discontinuities in rock masses from 3D point clouds *Eng. Geol.* 265 105442
- Lato M, Vöge M (2012) Automated mapping of rock discontinuities in 3D LIDAR models. *Int J Rock Mech Min Sci* 53: 150-158.
- Mauldon M, Dershowitz W (2000) A multi-dimensional system of fracture abundance measures. *Geological Society of America Abstracts with Programs* 32 7 A474
- Nironen M (2024) Geological Unit Report GTK. Geological Survey of Finland, code 211380.
- Riquelme AJ, Abellán A, Tomás R (2015) Discontinuity spacing analysis in rock masses using 3D point clouds. *Engineering Geology* 195, 185-195, <https://doi.org/10.1016/j.enggeo.2015.06.009>
- Riquelme AJ, Abellán A, Tomás R, & Jaboyedoff M (2014) A new approach for semi-automatic rock mass joints recognition from 3D point clouds. *Computers & Geosciences* 68, 38–52, <https://doi.org/10.1016/j.cageo.2014.03.014>
- Riquelme AJ, Tomás R, Cano M, Pastor JL, Abellán A (2018) Automatic mapping of discontinuity persistence on rock masses using 3D point clouds. *Rock Mech. Rock Eng.* 51 (10), 3005–3028, <https://doi.org/10.1007/s00603-018-1519-9>
- Umili G, Ferrero A and Einstein HHH (2013) A new method for automatic discontinuity traces sampling on rock mass 3D model *Comput. Geosci.* 51 182–92
- Uotinen L (2018) Prediction of stress-driven rock mass damage in spent nuclear fuel repositories in hard crystalline rock and in deep underground mines. Doctoral dissertation at Aalto University, Finland. <https://aaltodoc.aalto.fi/handle/123456789/30729>
- Zhang L, Einstein HH (2000) Estimating the intensity of rock discontinuities. *Int J Rock Mech Min Sci* 37:819–37.